Lithology and Mineral Resources, Vol. 39, No. 5, 2004, pp. 468–479. Translated from Litologiya i Poleznye Iskopaemye, No. 5, 2004, pp. 539–551.

Transformation of Hydroxyapatite of Bone Phosphate from the Ocean Bottom during Fossilization

J. G. Nemliher[1], G. N. Baturin[2], T. E. Kallaste[1], and I. O. Murdmaa[2]

[1] *Institute of Geology, Tallinn Technical University, Estonia avenue 7, Tallinn 10143, Estonia*
[2] *Shirsov Institute of Oceanology, Russian Academy of Sciences, Nakhimovskii pr. 36, Moscow, 117997 Russia*
e-mail: murdma@ocean.ru, murdmaa@mail.ru

Received June 6, 2003

Abstract—Samples of Recent–Miocene fish and marine mammal bones from the bottom of the Atlantic and Pacific oceans and Miocene Maikop deposits (Transcaspian region) are studied by the X-ray diffraction (XRD) technique combined with the chemical and energy-dispersive (EDX) analyses. Changes of lattice parameters and chemical composition of bioapatite during the fossilization and diagenesis suggest that the development of skeletal apatite proceeds from the dahllite- type hydroxyapatite to the francolite-type carbonate-fluorapatite. It is assumed that a jump-type transition from dahllite to francolite during the initial fossilization reflects the replacement of biogeochemical reactions in living organisms, which are subject to nonlinear laws of nonequilibrium thermodynamics, by physicochemical processes according to the linear equilibrium thermodynamics.

In general, apatites include a group of minerals with the common formula

$$(Ca, Na, Mg)_{10}(PO_4)_6(CO_3)_x(OH, F, Cl)_y,$$

which is characterized by a wide range of isomorphous substitutions. The isomorphism is principally related to the presence of carbonate-, halogen- (F, Cl) and OH-ions in the crystal lattice. Minor elements, such as Sr, V, S, and others, are also typical for the apatites (Nriagu, 1984).

Sedimentary and skeletal apatites are mainly represented by the fluorcarbonate-apatite (sedimentary) and hydroxyfluorcarbonate-apatite (skeletal) modifications. The first (francolite-type) apatite group is genetically related to the authigenic phosphate formation in upwelling zones (Baturin, 1978) and the diagenetic alteration of skeletal phosphates. The second group is represented by skeletal (dahllite-type) apatites, in the crystal lattice of which fluorine- carbonate-ions are supplemented with hydroxyl ions.

An empirical functionality of lattice parameters on the carbonate ion content has been found for the isomorphic series of francolite-type apatites (Gulbrandsen, 1970; Schuffert *et al.,* 1990). The relations between chemical composition and lattice parameters for dahllite-type apatites are much more complicated. However, one can observe a nearly linear function between the lattice parameter *a* and OH content. Unlike the francolite-type apatite, the dahllite-type modification is characterized by both specific chemical composition and poor crystallinity, mainly owing to tiny dimensions of crystallites of the skeletal apatite (Nemliher *et al.,* 1997). It should be pointed out that we failed to synthesize *in vitro* the skeletal mineral found *in vivo.*

It is noted that the reduction of lattice parameter *a* prevails during the fossilization of the skeletal apatite. This is believed to be caused by the substitution of OH and orthophosphate ions for F- and carbonate-ions, respectively (Lucas and Prévôt, 1991). However, attempts to model the transformation of dahllite into francolite (based on lattice parameters values and apatite structure) carried out by the authors suggested the absence of any continuous transitions between these minerals.

This work is aimed to study the character of hydroxyapatite transformation in fish and marine mammal bones from the ocean bottom during early stages of fossilization by means of the XRD and chemical analyses.

MATERIALS AND METHODS

The studied material is represented by 19 fragments of fish and marine mammal skeletons taken from the bottom of Atlantic and Pacific oceans during cruises of research vessels of the Shirshov Institute of Oceanology, Russian Academy of Sciences. The materials comprise rib and skull bones of marine mammals, vertebrae and teeth of fishes, whale earbones (otoliths), and trihedral fish bones described in literature as dreikanters (Bremner, 1980).

We also studied phosphatic brachiopod shells from the Namibian shelf, two bone samples from the Transcaspian Maikop deposits, and four samples of oceanic phosphorites (including three phosphorite nodules from the coastal upwelling zone and one sample of

0024-4902/04/3905-0468 © 2004 MAIK "Nauka/Interperiodica"

Table 1. Coordinates and depths of sampling stations

Station no.	Coordinates	Depth, m	Material
		Atlantic Ocean	
2048	22°08′ S, 13°58′ E	76	Holocene phosphorite nodule
2046	22°40′ S, 14°15′ E	87	Holocene phosphatized coprolite, fragments of fish bones
144	22°56,7′ S, 13°48.2′ E	148	Bones of fishes and mammals
L-412	25°15.9′ S, 14°03.0′ E	199	The same
1529	19°15.5′ S, 12°06.5′ E	232	Tuna vertebra
1535	18°58.8′ S, 12°11.7′ E	180	Skull of marine sheatfish
351	15°06.5 S, 13°46.0′ E	283	Whale skull
217	17°28.0′ S, 10°30.0′ E	140	Whale rib
1006	19°20.8′ S, 12°15.2′ E	200	The same
		Pacific Ocean	
250	21°08′ S, 70°21′ W	150	Fish and whale bones
3802	3°17′ S, 172°52.3′ W	5329	Whale otolith
5159	7°35.5′ N, 161°55.8′ W	4916	The same
6333	12°54′ S, 160°44′ W	3620	Shark teeth and whale otoliths
6349	18°30′ N, 175°28′ W	2280	Phosphatized limestone

phosphatized limestone from a Pacific seamount) for comparison. The sampling sites are given in Table 1. Owing to the absence of precise coordinates, sampling sites are not shown in the table for samples AK-1 (teeth of a living shark caught in the central Pacific during an expedition), MK-2 (shark tooth from the Maikop deposits), MK-3 (dolphin vertebra from the Maikop deposits), and phosphatic brachiopod shells from the Namibian shelf (DN 2, DN 1a, and DN 3).

Most of the studied samples were taken from phosphate-bearing sediments of the Namibian and Chilean shelves described in (Baturin, 1978). Samples from the Maikop deposits were presented by A.V. Kochenov. They were taken from the metalliferous bone breccia deposit (Kochenov and Stolyarov, 1996; Sharkov, 2000).

Elemental composition of samples was determined by classical chemical analyses in analytical laboratories of the Shirshov Institute of Oceanology (Moscow) and the Far East Geological Institute (Vladivostok). We should note that control analyses of fluorine revealed some underestimation of the F content in several samples analyzed in the Far East Geological Institute. However, this does not considerably affect the general regularities in fluorine behavior during the bone apatite fossilization considered here.

The X-ray diffraction (XRD) studies were performed at the Institute of Geology (Tallinn Technical University) on a HZG4 diffractometer using Fe-filters and Co radiation.

Samples for the XRD analysis were powdered in a mortar. The powder was mixed with about 5–10% of quartz (correction standard) and some drops of alcohol. The obtained preparation was spread as a patch, 15–20 mm in diameter, on a slide. The samples were scanned at a step of 0.02° within the range of 29°–41° and 54°–64°, which contained 15 apatite and two quartz reflections.

The least-squares fitting method was applied for processing the measurement results using standard software. The shape of the $K\alpha_1$ reflection is described by the function

$$I(2\theta) = I\,\max(1 + ((2\theta - 2\theta\max)/w)^2)^{-b};$$

where $I(2\theta)$ is the intensity at point 2θ, I max is the intensity at the peak (2θ max), w is the width parameter, and b is the peak shape parameter.

Thus, each reflection is determined by four parameters (location, height, width, and shape), the values of which were obtained by fitting the model onto the measured profile. In the case of low-crystalline recent bioapatite, most of the reflections are greatly overlapping (e.g., 211, 112, 300, and 202). Therefore, the application of approximation with a large number of the degree of freedom often yields parameter values that have no significance for the object under study; i.e., the numerical values obtained are solely generated by the mathematical method. In such cases, the number of the degree of freedom was reduced. Instead of variation of a single XRD reflection position within the group of reflections, we varied in the course of fitting the lattice parameters, which determine the overall position of the group of reflections. A linear angle correction by two quartz reflections was used. In order to eliminate the background and its inclination, we also used the linear

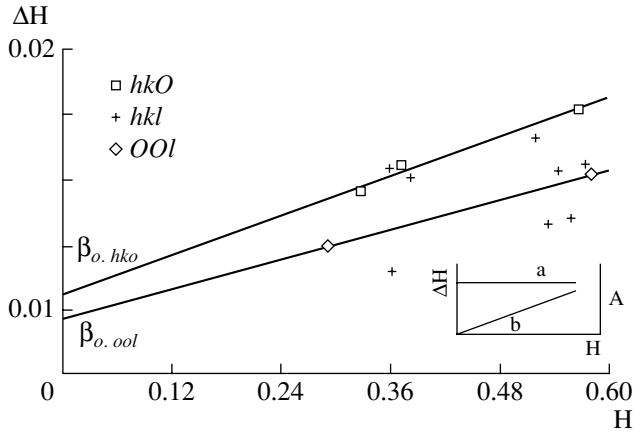

Fig. 1. Dependence of the node-size of reciprocal lattice *H* on the modulus of the reciprocal lattice vector *H*. (A) The Iveronova and Revkevich model (1978) demonstrating the dependence in two extreme cases: (a) widening is caused only by small dimensions of crystallites; (b) widening is caused only by strain. (B) Illustration of the model for reflections *hko, hkl, ool* in the fish bone sample 4-12P.

approximation, during which the intensities of terminal segments of the measured angle ranges were considered as free parameters, which were changed together with the intensity variation over the XRD pattern. The reflection width was related to the crystallite size using the model by Iveronova and Revkevich (1978) (Fig. 1). Application of this model is shown on the basis of sample 4-12-P (Fig. 2). Although application of the model is not exactly correct here, but it allows us to derive relevant information for the description of the studied objects and their comparison. In the figure, β is the integrated half-width of the apatite $K\alpha_1$ reflection in the reciprocal-lattice scale calculated by the formula $\beta = B - b$, where β and *b* are the measured integrated half-widths of apatite and quartz reflections, respectively; i.e., the correction of instrumental widening is applied according to the width of the quartz reflection.

Crystallite dimension in a particular lattice direction of vector H_1 is estimated from the reciprocal value of β_0: $D = \beta_0^{-1}$. Parameter of the reflection shape can be attributed to the statistical distribution of crystallite dimension parameters. If all crystallites are of the uniform size and strains are absent, the reflection profile resembles the Gaussian distribution. If the reflection shape is represented by sharp peak and wide base (low values of the profile-shape parameter), the sample obviously consists of a mixture of large and small crystallites.

Strain (content of lattice imperfections) in the particular lattice direction of vector *H* is estimated from the slope of linear approximation of values in the same direction. In this work, the strain was estimated in two directions: alongside the hexagonal prism $[\Delta d/d)_{ool}]$ and in perpendicular direction $[(\Delta d/d)_{hko}]$. Values of lattice parameters were calculated by positions of $K\alpha_1$ reflections using the least-squares method.

The carbonate-ion content in the carbonate-fluorapatite series was determined using the equation in (Gulbrandsen, 1970; Schuffert *et al.*, 1990):

$$[CO_3] = f(a, c) = r(2\theta_{max(hko)}2\theta_{max(ool)}) + k,$$

where k and r are the empirically found parameters of the functional dependence. According to (McConnell, 1973), the carbonate content in the apatite lattice ranges from 0% (pure F-apatite) to 6% (francolite).

RESULTS

Chemical Composition of Bones

As shown by bulk chemical analyses (Table 2), the P_2O_5 content in bone samples from the ocean bottom ranges from 19.00 to 33.92%. Minimal values (19–23%) characterize porous samples with inclusions of terrigenous material and biogenic carbonate, as evidenced by increased Al_2O_3, SiO_2, and CO_2 contents. The maximal P_2O_5 content is recorded in the tooth enamel of a Tertiary shark from the Pacific bottom.

Examination of bone samples of the same type and different degrees of fossilization revealed the following trend. The content of constitutional water (H_2O^-) decreases and the content of fluorine bound with phosphate (i.e., F/P_2O_5) increases with increase in fossilization. In several samples taken from the open ocean bottom, where oxidizing conditions exist, accumulation of iron and manganese hydroxides in the Tertiary shark tooth is also maximal (6.14% Fe and 3.98% Mn).

The organic carbon content in the studied skeletal remains varies from 0.39% (Tertiary shark tooth from the Pacific pelagic area) to 11.04% (tooth of a living shark). The C_{org} content is lower in phosphorites (0.17–1.50%). In general, the C_{org} concentration decreases with increase in the fossilization degree, although any distinct reverse relationship with fossilization indicators, such as P_2O_5 and F contents, is absent for the studied samples. It is known that phosphorus associates with organic matter, on the one hand, but it is present in the enclosing sediments filling voids in the bone tissue, on the other hand. Therefore, data on the C_{org} content (Table 2) allow us to only tentatively judge about the relationship between organic and mineral (apatitic) constituents of the bone material. Nevertheless, the *post mortem* alteration and fossilization of bone remains are obviously accompanied by the decay and removal of organic matter from the bone tissue and the corresponding increase in the proportion of mineral (phosphatic) component.

The bone pores contain a considerable and hardly determinable admixture of biogenic carbonate of enclosing sediments and authigenic carbonate. Therefore, we cannot directly relate the CO_2 data in Table 2 to carbonate-ion content in the bone apatite. Nevertheless, we can ascertain that the CO_2 content in some ancient (fossilized) varieties of bone remains (shark teeth, dreikanters, and whale bones) is higher relative to

Table 2. Chemical composition of studied samples

Sample no.	Sample characteristics	P_2O_5	CaO	MgO	Na_2O	K_2O	SiO_2	TiO_2	Al_2O_3	Fe_2O	MnO	H_2O^-	H_2O^+	CO_2	C_{org}	Total SO_3	F
AK-1	Living shark teeth	27.83	40.56	1.41	0.82	0.04	1.00	0.14	0.40	0.29	0.04	1.91	8.82	1.72	11.04	3.51	0.33
20464	Merluse teeth	20.92	39.87	1.71	2.29	0.09	1.62	0.14	0.70	0.01	0.00	1.69	4.27	–	–	1.65	0.69
6333-31	Teeth of Tertiary sharks, Pacific Ocean	28.04	39.34	0.85	1.15	0.41	4.11	0.62	6.4	6.14	3.98	1.40	9.38	0.73	0.39	–	0.80
6333-32	The same	33.92	44.13	0.77	1.45	0.18	1.31	0.52	0.55	4.10	2.46	0.30	8.01	–	–	–	1.10
MK-2	Shark teeth from Maikop clay	26.89	48.36	1.05	1.00	0.12	1.20	0.20	0.95	3.30	0.06	0.31	2.44	2.78	0.92	2.57	1.35
250-D	nonfossilized	25.69	47.61	0.87	0.55	0.13	1.31	0.00	0.30	0.21	0.00	0.82	3.17	3.13	–	3.50	1.39
250-D	Fossilized	27.88	48.70	0.81	1.45	0.12	2.90	0.00	0.87	0.72	0.00	0.30	5.50	4.88	–	3.88	1.58
250-PR	Slightly fossilized	24.70	43.08	1.12	1.73	0.16	1.81	0.09	0.92	0.00	0.00	2.30	7.02	12.83	1.62	2.98	1.33
412-P	The same	19.00	56.55	1.11	0.92	0.10	0.91	0.05	0.07	0.78	0.00	0.71	3.50	9.00	1.97	2.00	0.95
144-K	Slightly fossilized	26.81	49.32	1.13	0.84	0.13	1.91	0.00	0.59	0.63	0.00	0.70	5.88	6.58	3.92	3.08	1.60
412-KR	More fossilized	22.22	57.90	1.35	1.11	0.09	1.26	0.05	0.83	0.97	0.00	0.42	2.55	10.56	–	0.00	1.44
1535	Skull bone of sheatfish	19.40	32.95	1.19	1.66	0.31	8.22	0.15	0.86	5.44	0.00	1.70	5.08	11.24	4.27	10.57	1.52
1529	Tuna vertebra	23.06	35.64	1.33	1.50	0.25	5.08	0.10	0.65	1.44	0.00	1.16	3.35	5.05	8.28	1.23	2.10
5159-1	Nonfossilized	32.49	47.71	0.73	1.72	0.00	0.80	0.09	0.00	0.20	0.07	0.30	7.71	7.51	0.48	0.00	–
6333-106	Moderately ferruginated	28.62	45.19	1.11	1.82	0.18	1.29	0.28	0.38	1.94	1.17	0.80	7.70	7.26	0.46	0.94	–
3802	Impregnated by Mn	25.68	41.64	1.52	2.21	0.52	3.31	0.19	1.32	0.07	3.64	0.70	8.82	5.05	–	0.95	–
1007	Slightly fossilized	27.60	40.05	0.14	1.35	0.00	1.23	1.10	0.00	2.08	0.06	2.46	13.37	5.35	6.60	1.41	1.33
250-KK	The same	20.01	35.81	1.26	2.47	0.33	10.23	0.00	3.48	0.76	0.00	2.78	11.00	8.44	-	2.18	1.58
1006	Moderately fossilized	29.52	46.92	0.09	1.29	0.19	1.20	0.15	0.27	2.20	0.00	0.60	7.18	5.81	1.12	5.08	2.66
217	The same	26.61	48.59	0.82	1.00	0.18	3.70	0.00	0.93	0.65	0.00	0.90	6.69	6.33	0.98	2.95	3.08
412-KM	Slightly fossilized whale skull bone	25.60	48.57	1.54	0.53	0.12	1.60	0.15	0.54	1.09	0.00	0.70	5.00	8.80	1.68	3.83	1.39
351-K	The same	28.62	42.60	1.20	1.27	0.13	1.24	0.10	0.18	2.00	0.00	1.43	7.39	5.22	2.98	4.30	2.40
MK-3	Dolphine vertebra from the Maikop clay	15.30	53.00	0.54	0.32	0.30	3.00	0.30	1.30	1.84	0.20	0.60	1.31	20.00	3.86	1.47	1.14
204b-12	Phosphatized coprolite, Holocene	30.45	49.0	1.32	0.38	0.05	0.30	0.02	0.20	0.1	0.01	–	2.97	6.14	1.08	2.07	2.96
2048-8	Phosphorite nodule, Holocene	29.97	48.7	1.51	0.22	0.05	0.20	0.02	0.20	0.1	0.01	–	3.31	6.36	0.17	1.95	3.19
412-F	The same, Pliocene	32.53	51.0	0.91	0.41	0.05	0.80	0.02	0.13	1.8	0.24	–	1.92	5.85	1.50	5.37	3.41
6349-1	Phosphatized limestone, Upper Cretaceous	23.00	550.4	0.29	1.3	0.36	1.62	0.044	0.60	0.41	0.13	–	–	10.17	0.22	–	–

Table 3. Parameters of elementary cell (Å) and calculated carbonate-ion content (%) in carbonate-apatites of studied samples

Sample no.	Parameter *a*	Parameter *c*	CO_3
Fish teeth			
AK-1	9.395	6.875	0.62
2046-4	9.381	6.889	1.3
6333-31	9.385	6.884	1.06
6333-32	9.379	6.884	1.18
MK-2	9.385	6.886	1.13
Average	9.385	6.886	1.19
Dreikanters			
250-D	9.367	6.885	1.42
250-DF	9.352	6.888	1.82
Average	9.360	6.886	1.62
Fish vertebrae			
250-PR	9.355	6.886	1.69
412-P	9.348	6.882	1.69
Average	9.351	6.884	1.69
Small fish bones			
144-K	9.349	6.892	2.00
412-KR	9.328	6.889	2.29
Average	9.338	6.890	2.14
Large fish bones			
1535	9.367	6.885	2.26
1529	9.352	6.889	2.46
Average	9.359	6.887	2.36
Cetacean otoliths			
6333-106[6]	9.396	6.904	1.46
5159-1	9.390	6.906	1.63
3802	9.362	6.901	2.04
Average	9.383	9.904	1.71
Fragments of Cetacean rib bones			
1007	9.372	6.889	1.46
250-KK	9.360	6.888	1.64
1006	9.339	6.895	2.27
217-K	9.332	6.894	2.41
Average	9.351	6.891	1.94
Large bones of Cetaceans			
412-KM	9.332	6.887	2.17
351-K	9.332	6.896	2.45
MK-3	9.349	6.894	2.07
Average	9.338	6.892	2.24
Brachiopod (lingulate) shells			
DN 2	9.385	6.871	0.67
DN 1Ä	9.380	6.873	0.82
DN 3	9.379	6.871	0.78
Average	9.381	6.872	0.76
Phosphorites			
2046-12	9.322	6.887	2.36
2048-8	9.325	6.886	2.27
412-F	9.329	6.889	2.28
6349-1	9.329	6.900	2.66
Average	9.326	6.890	2.39

their younger (weakly fossilized) analogues. This likely reflects an increase of the carbonate-ion content in apatite during fossilization. However, reverse examples are also observed. The high carbonate content in the studied phosphorite samples apparently results from the presence of carbonate minerals.

The constitutional water (H_2O^-) content in the studied bone samples varies from 0.30 to 2.78% (Table 2). It is rather unclear, how much these data reflect the content of hydroxyl-ion in the apatite. We shall return to this issue later, when XRD results of the bone apatite are considered. Here, we only note that if the difference in fossilization degree (age) of various bone remains is reliably determined, the younger (nonfossilized) varieties apparently contain more of the constitutional water than their ancient analogues. For example, the H_2O^- content is 1.97% in the living shark teeth (sample AK-1) and only 0.30–0.31% in the Tertiary shark tooth from the Pacific bottom (sample 6333-32) or the Maikop deposits (sample MK-2). In whale ribbon bones, the H_2O^- decreases from 2.46–2.78% in the apparently low-fossilized varieties to 0.60–0.90% in the moderately fossilized ones.

Lattice Parameters of the Bone Apatite

Values of lattice parameters *a* and *c*, as well as the calculated carbonate content of studied material, are presented in Table 3. Their relationship is shown in Fig. 2. For comparison, data on apatite of recent (subfossil) brachiopod (lingulate) shells from the coastal zone of Namibia (Nemliher and Kallaste, 2002) are also plotted in Fig. 2.

As shown in Fig. 2, the lattice parameter *a* variation range (9.33–9.40 Å) significantly exceeds that of parameter *c* (6.88–6.90 Å for most samples). Despite the large scatter of values, one can outline some regularities, especially if data on certain separate groups of bone, rather the whole set of samples, are examined.

Data points of all shark teeth with the lattice parameter *a* exceeding 9.375 Å are plotted on the right side of the diagram, while data points of the living shark tooth (sample AK-1) fall into the lowermost right field with the highest *a* (9.394 Å) and the lowest *c* (6.875 Å) values obtained for the set of bone apatite samples (Table 3). Tertiary shark teeth data tend to group around values of *a* = 9.379–9.385 Å and *c* = 6.883–6.888 Å, displaying a weak trend of decrease in parameter *a* and increase in *c* relative to the living shark tooth. This reflects changes in the crystal structure of skeletal apatite during the fossilization and diagenesis as a result of increase in the carbonate-ion content.

In terms of apatite lattice parameters, cetacean bones can be divided into two distinct groups (Fig. 2, Table 3). The apatite of cetacean earbones shows the highest *c* values (6.901–6.905 Å) and a wide variation of *a* value from 9.361 Å (the Pacific pelagic clay sample impregnated with manganese hydroxides) to as

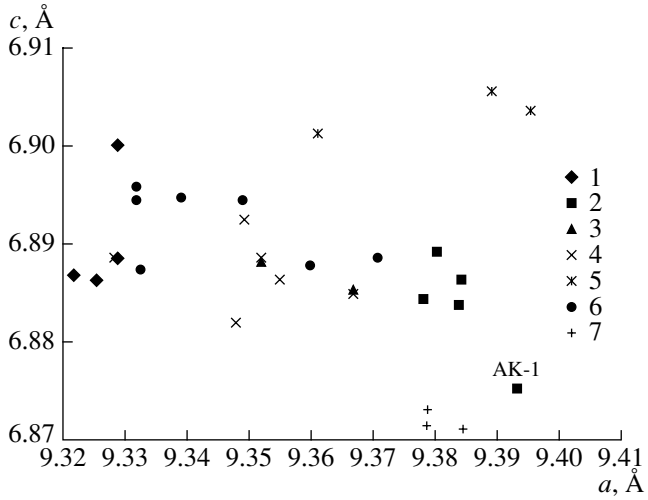

Fig. 2. Relationship between lattice parameters *a* and *c* of apatite in the studied samples. (1) Phosphorites; (2) fish bones; (3) dreikanters; (4) fish bones; (5) whale otoliths; (6) whale bones; (7) brachiopod (lingulate) shells (*Discinisca*).

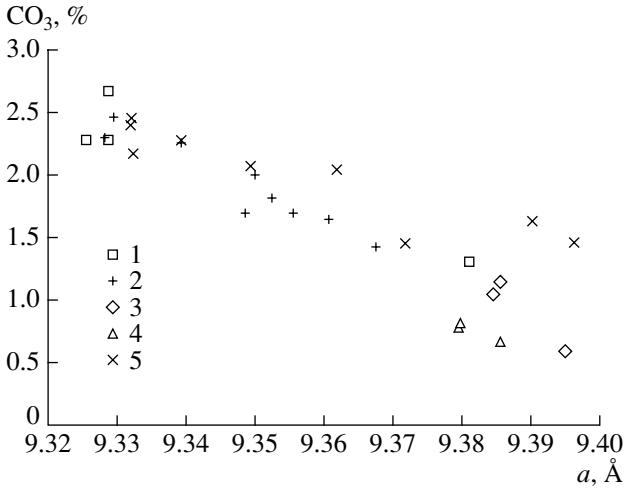

Fig. 3. Relationship between lattice parameter *a* and calculated carbonate-ion in phosphate. (1) Phosphorites; (2) fish bones; (3) fish teeth; (4) brachiopod (lingulate) shells; (5) mammals bones.

much as 9.396 Å (a moderately ferruginated sample from the Manihiki Plateau, South Pacific). The *a* value demonstrates a wider variation in the bone apatite of cetacean rib and scull fragments ranging from values close to those for the oceanic phosphorite apatite (9.331–9.332 Å) to 9.71 Å. Meanwhile, the *c* value appears to be relatively stable. The calculated carbonate-ion content in the apatite lattice of cetacean earbones (1.46–2.04%, average 1.71%) is considerably higher relative to the shark teeth, but it is commonly lower than that in cetacean rib and scull fragments (1.46–2.41%, average 1.94%).

Data points of bony fishes (*Teleosta*) fall into the left and middle fields of the plot (Fig. 2), roughly continuing the decreasing trend of parameter *a* and increasing trend of parameter *c* revealed for the shark teeth apatite. The phosphorite field at the left upper end of this trend (Fig. 2) includes the apatite of small fish bones (a = 9.328 Å, c = 6.888 Å) from the Namibian upwelling zone (sample 412-KP), with a high carbonate content (2.29%). Data point of nonfossilized dreikanters and scull fragments of marine sheatfish from the Namibian shelf (a = 9.367 Å, and c = 6.885 Å) fall into the right lower corner of the plot. The calculated carbonate-ion content in the apatite of dreikanters is low (1.42–1.82%). However, this value is slightly higher in their fossil specimens. Large fragments of teleost bones (scull of marine sheatfish and tuna vertebra) are characterized by remarkably higher carbonate contents (2.26–2.46%).

Thus, despite the considerably random scatter of lattice parameter values, one can ascertain that the *a* value decreases from the bone apatite of living shark teeth to the fossilized Tertiary varieties and further from the fresh teleost bones from the Namibian shelf to their fossilized varieties. The *a* value of the apatite in the latter fossilized variety is close to that of fossilized bones of cetaceans and the studied samples of nonskeletal phosphorites (9.321–9.328 Å, average 9. 325 Å). Variations in the *c* value of skeletal apatite in most of the studied samples show a narrow range (6.883–6.896 Å), except for the living shark teeth (6.875 Å) and the apatite of whale earbones (>6.9 Å). Data points of the apatite of subfossil lingulate shells (Nemliher and Kallaste, 2002) are clustered in the lower right corner of the plot (away from those of the bone apatite) and characterized by higher *a* values and lower *c* values (Fig. 2).

The inverse linear dependence between *a* and the calculated CO_3 content in apatite (Fig. 3) is predetermined by the calculation formula and the weak influence of *c* variations on the carbonate-ion content. However, one can observe a compact group of low *a* values (9.325–9.340 Å) and, correspondingly, high carbonate-ion contents (2.2–2.5%) in the left upper part of the plot (Fig. 3) increase in the scatter of data points in the right lower corner including shark teeth, whale otoliths, and lingulate shells.

The studied apatite samples show a variable crystallinity (Table 4). The applied calculation method did not yield satisfactory results for all studied samples. However, both "fresh" and sufficiently fossilized skeletal apatites can generally be well described by the used model.

DISCUSSION

Based on analyses of the skeletal apatite from different groups of recent vertebrates (Nemliher *et al.*, 1997), we can affirm that the skeletons consist of the F–OH-carbonate-apatite (hydroxyfluorapatite-carbonate) with a variable carbonate-ion content. Results of our work suggest that the *post mortem* alteration of the skeletal

Table 4. Dimension of crystallites of the phosphate mineral along *hk0* (L*a*, Å) and *001* (L*c*, Å) and crystal lattice strain value

Sample no.	L*a*	L*c*	L*a*/L*c*	$(\Delta d/d)_{hk0}$	$(\Delta d/d)_{001}$	$(\Delta d/d)_{hk0}/(\Delta d/d)_{001}$
Fish bones						
AK-1	2232	333	0.149	0.006	0.003	1.933
6333-31	799	3115	3.897	0.004	0.003	1.059
2046-11	132	121	0.922	0.065	0.008	7.924
MK-2	–	–	–	0.012	0.001	8.042
Dreikanters						
250-D	601	1074	1.788	0.002	0.001	1.788
250-DF	254	609	2.068	0.009	0.004	2.184
Fish vertebrae						
250-PR	139	360	2.596	0.000	0.000	1.056
412-P	254	359	1.415	0.016	0.012	1.340
Small fish bones						
144-K	168	224	1.338	0.005	0.000	11.339
412-KR	877	1883	2.147	0.012	0.006	2.179
Cetacean otoliths						
6333-10b	873	546	0.625	0.003	0.002	2.758
5159-1	855	1370	1.603	0.005	0.004	1.797
3802	525	518	0.987	0.004	0.004	1.194
Fragments of Cetaceans rib bones						
1007	–	–	–	0.021	0.005	4.047
250-KK	206	179	0.869	0.013	0.000	40.935
1006	391	469	1.201	0.010	0.005	2.147
217-K	1681	315	0.188	0.009	0.003	2.776
Large bones of Cetaceans						
412-KM	13699	1248	0.091	0.015	0.005	2.758
351-K	225	339	1.509	0.010	0.005	1.928
Brachiopods						
DN 2	1186	372	0.313	0.013	0.001	20.000
DN 1A	276	326	1.179	0.009	0.000	22.886
DN 3	250	615	2.458	0.005	0.004	1.238
Phosphorites						
2046-12	536	617	1.152	0.003	0.001	2.644
412-F	282	1009	3.582	0.004	0.004	1.024

Note: (–) Not determined.

apatite primarily leads to reduction of parameter *a* relative to the initial material (unaltered bioapatite). The recrystallization of apatite is related to decrease in the hydroxyl-ion content. This process ends with the transition to francolite-type apatite. The rate and scale of such alterations depend on the chemical composition of the initial material and the density of bone tissue subjected to alteration. The *a* value is ~9.44 Å in the mammal skeleton apatite and ~9.40 Å in the living shark teeth (Nemliher *et al.*, 1997). Moreover, whale otoliths contain less organic matter than the living shark teeth. Therefore, the transformation rate of their apatite is lower. This explains the rather high *a* values obtained for some subfossil whale otoliths and the distribution pattern of apatite lattice parameters shown in Fig. 2.

Division of the studied bone samples into groups according to their morphological features and taxonomy revealed a noticeable decrease in the *a* value with increase in the fossilization of bones, whereas the *c* value can remain stable or change in both directions (Fig. 4).

Data on lattice parameters of the apatite in subfossil brachiopod *Discinisca* shells (Nemliher and Kallaste, 2002) allow us to assume that alteration of the skeletal apatite also commences at the subfossil stage. This can be considered a preliminary condition for the skeleton preservation in the fossil state. Relative to other skeletal apatites, the lingulate apatite is marked by a lower OH-ion content (and the lowest *a* values). Hence, we can suggest its most rapid *post mortem* alteration relative to bioapatites of other taxons.

If a large set of samples (e.g., teleosts and mammals) is analyzed, one can see an individual trend within the data group demonstrating dependence of parameter *a* on the carbonate-ion content (Fig. 4). We interpret this as evidence of a partial preservation of the primary (taxon-specific) chemical composition during fossilization. Therefore, we can assume that, despite different fossilization rates, the primary biogenic apatite preserves some recognizable primary features of its lattice.

Based on the above data, we consider the studied samples of skeletal fragments as a preliminarily fossilized (francolite-type) material located at different stages of diagenesis. In such cases, the distinction of apatite lattice parameters from those assumed for the primary material reflects the intensity of diagenetic alteration.

The comparison of apatites of Cretaceous–Paleogene phosphorites from Pacific seamounts (Murdmaa *et al.*, 1995) with the Holocene phosphate nodules and coprolites from the coastal upwelling zones (Fig. 2) showed that the ancient phosphorites are characterized by higher *c* values and better crystallinity. Such distinction can be related to their different formation mechanisms and diagenetic alteration degrees. Phosphorites on seamounts formed due to the metasomatic replacement of biogenic limestones by fluorapatite in the oxidizing environment within the oceanic pelagic regions. Such phosphorites represent an ultimate diagenetic product. In contrast, the young phosphorites from the upwelling zone formed in a reducing environment of the organic-rich diatom ooze with intense bacterial activity at an early stage of diagenesis (Baturin, 1978). At the same time, both types of nonskeletal phosphorites are characterized by low *a* values (Fig. 2) and high carbonate-ion contents in the apatite lattice (Fig. 3).

Data on variations in the apatite lattice parameters relative to the geological age are summarized in Fig. 5. The skeletal apatite of recent animals is compared with the Holocene phosphorites from the upwelling zone in Fig. 5a. Lattice parameters of the Cenozoic fossils and phosphorites (data from this study) are plotted in Fig. 5b. Figure 5c shows data on the Paleozoic shell phosphorites, various fishes, and nodular phosphorites (Nemliher and Puura, 1996; Nemliher *et al.*, 1996). As follows from Fig. 5, the *a* value of the skeletal apatite substantially decreases with the development of diagenesis. Ultimately, the apatite reaches a stable state

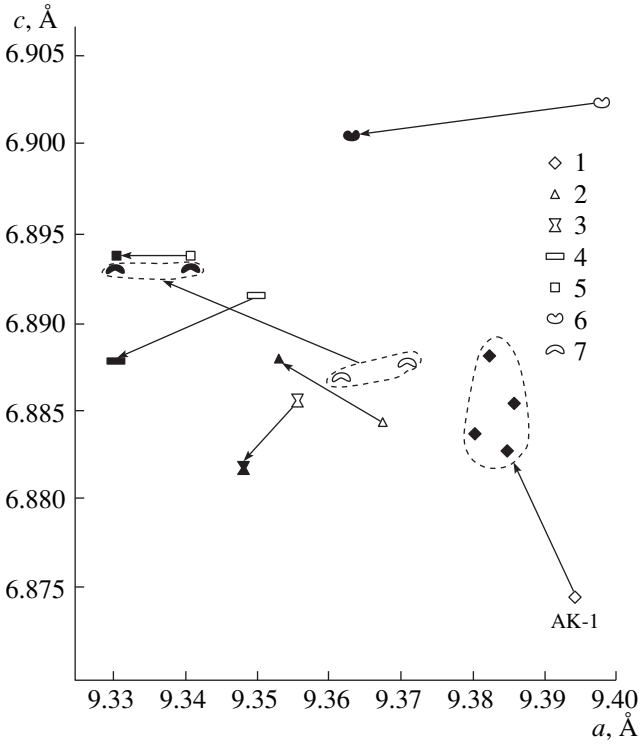

Fig. 4. Lattice parameters of apatite for sample groups vs. the fossilization degree. Fish bones: (1) teeth, (2) dreikanters, (3) vertebrae, (4) small bones, (5) large bones; Cetaceans bones: (6) otoliths, (7) ribs. Open symbols indicate relatively fresh bones; filled symbols, fossilized ones.

and is transformed from carbonate-fluorapatite into fluorapatite with very low carbonate-ion content (Fig. 5c). This process is likely related to the intensity of diagenesis and catagenesis rather than the age.

Thus, our studies confirm that the *a* value of the skeletal apatite regularly decreases during its diagenetic alteration. This is probably related to the replacement of OH- and orthophosphate-ions in the dahllite-type bioapatite of the bone tissue (or shell) in living organisms by F- and carbonate-ions, respectively (Lucas and Prévôt, 1991). However, attempts to construct the dahllite-to-francolite isomorphic series of skeletal apatites suggested the absence of any continuous transitions between these phases. If the theoretical assumption about a jump-type transformation of the crystal lattice of skeletal apatites corresponds to natural processes, it is necessary to explain both the wide scatter of lattice parameters values of the studied skeletal apatites and the appearance of individual trends of their changes in different groups of skeletal apatites during fossilization (Figs. 2, 5).

In order to compare data on lattice parameters with characteristics of chemical composition of the skeletal and nonskeletal apatites, we used the calculated value of elementary cell volume (*V*) that simultaneously takes into account variations in both lattice parameters. It is known from previous investigations that values of apa-

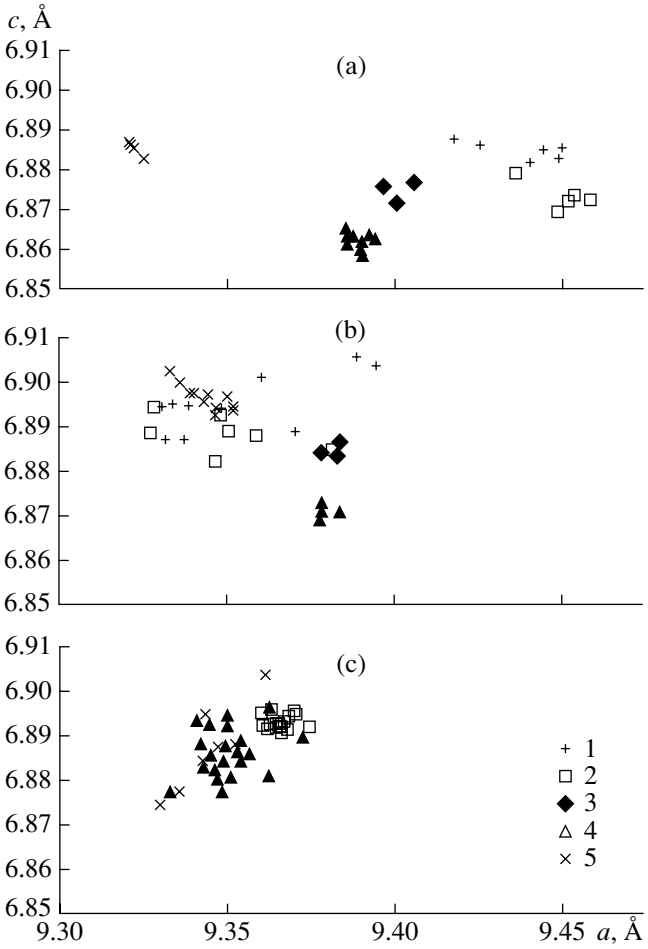

Fig. 5. Changes of apatite lattice parameters with geological time in genetically different phosphates. (a) Recent bones and phosphorites from upwelling zones; (b) Cenozoic fossil bones and phosphorites; (c) Paleozoic shell and nodular phosphorites and fish remains. (1) Mammal bones; (2) fish bones; (3) fish teeth; (4) lingulate shells; (5) phosphorites from upwelling zones.

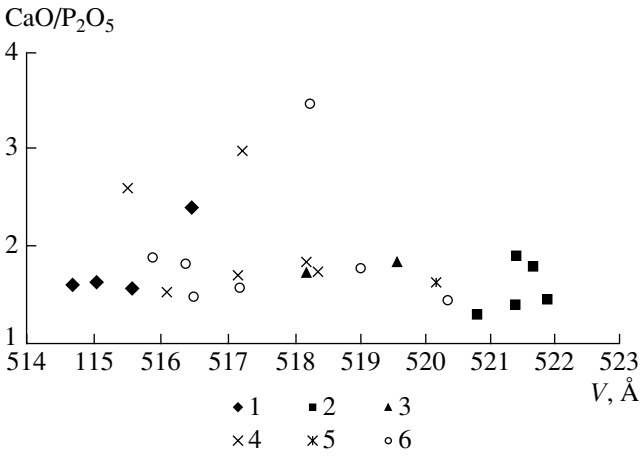

Fig. 6. Dependence of elementary cell volume (V) on the CaO/P_2O_5 ratio in apatites. (1) Phosphorites; (2) fish teeth; (3) dreikanters; (4) fish bones; (5) whale otoliths; (6) whale bones.

tite lattice parameters represent an integral function not only of its chemical composition (McConnel, 1973), but also of the disposition of ions in the crystal lattice (Elliot, 1994). Values of both apatite lattice parameters may be presented as the volume of elementary cell of the hexagonal system: $V = 0.86a^2c$. This allows us to reduce the variability of crystal lattice to variations of a single parameter that may easily be compared with the chemical composition.

As shown in Fig. 6, CaO/P_2O_5 values are not related to the elementary cell volume. In most samples, the ratio ranges from 1.2 to 2 at extremely wide variations of V. The ratio is more than 2 only in four samples (with the maximal value up to 3.45 in the whale otolith from the Maikop deposits), probably, owing to an admixture of enclosing sediments. This is indicated by the low phosphorus content in these samples. Maximal values of elementary cell volume are typical of the shark teeth apatite, whereas the minimal values are detected in ancient phosphorites. We have to note that the CaO/P_2O_5 ratio in the studied phosphorites correspond well to the published data (Bremner and Rogers, 1990; and others).

Crystal chemistry of carbonate-apatites and its relationship to crystallographic constants have been investigated for a long time (McClellan and Lehr, 1969). If one assumes that the replacement of phosphate-ion by carbonate-ion is responsible for changes in lattice parameters and takes into consideration data in (McConnell, 1973), the composition of carbonate-fluorapatites should much more drastically change within the range of elementary cell volume variations shown in Fig. 6. Moreover, based on data in (Gulbrandsen *et al.*, 1984; Nathan, 1984), we may suggest that the replacement of orthophosphate-ion by carbonate-ion in the apatite crystal lattice leads to decrease of the Ca contribution to the stoichiometric ratio Ca/P = 10/6 and the respective decrease of the CO_3 proportion.

Such a relationship should obviously shift the CaO/P_2O_5 variation trend toward higher V values in Fig. 6. However, we actually see an opposite pattern.

Nevertheless, it is obvious that the relationship Ca/P < 10/6 is only observed in the francolite-type apatites, but it is not recorded in the varieties containing OH-ion. Moreover, recent data indicate a duplex CO_3 position in apatite (Elliot, 1994).

Therefore, we explain the wide scatter of data points in Fig. 6 as a result of the following three factors: (a) positive correlation of Ca/P and V in the apatite of phosphorites; (b) appearance of Ca-containing admixtures during diagenesis; and (c) manifestation of negative relationship between the lattice parameters during *post mortem* alteration of bioapatites.

The relationship between the elementary cell volume and fluorine content in the studied samples demonstrates a distinct reverse trend and significant data scatter (Fig. 7). Since the diffractometry did not reveal the presence of fluorite in any of the studied samples, we can ascertain that the fluorine is totally incorporated in the apatite lattice. Therefore, the decrease of V with increasing F content may be explained as a result of OH-ion removal from the skeletal apatite lattice and occupation of its position by F-ion, i.e., transition from the dahllite-type hydroxyfluorapatite to the francolite-type carbonate-fluorapatite.

Data points of fish teeth, including the living shark teeth with the maximal V and minimal F contents are located at the right lower end of this trend. Teeth of the living shark may be considered an example of the primary dahllite-type skeletal apatite unaffected by francolitization. Like in the Ca/P plot (Fig. 6), data points of apatite from phosphorites with the maximal F content and minimal elementary lattice cell volume are located at the left end of the trend. These results correspond to the data reported by Dahma and Risness (1999).These data explain the difference in contents and positions of OH- and F-ions in the shark teeth enamel and phosphoritic apatite. Let us remember that the living shark teeth are characterized by high H_2O^- concentrations and the minimal carbonate content among all samples (Tables 2, 3).

Data points of apatites of fossilized whale bones and large fish bones approach the phosphorite field in Fig. 7. They are also characterized by the lack of H_2O^- (i.e., of hydroxyl-ion). Intermediate values of elementary cell volumes (F 1.0–1.2%) located between the extremum values characterize the majority of fish and cetacean bone samples.

We have to keep in mind that the stoichiometric apatite composition must contain 2 mol% of (OH + F + Cl). Therefore, we interpret F-poor apatites as OH-rich varieties. The lack of any distinct negative correlation between constitutional water and F content (Table 2) is presumably related to difficulties in the determination of the OH-ion content in the apatite lattice by means of routine chemical methods.

This interpretation is supported by the noticeable increase in the *a* value as a result of the occupation of an additional anion position by the OH-ion (Figs. 3, 7). Therefore, we believe that the F content in the apatite lattice best characterizes the diagenetic alteration degree of bioapatites.

Based on the data presented above and the hypothesis about the absence of intermediate phases between dahllite and francolite, we suggest that the francolitization of skeletal apatites is related to recrystallization rather than the metasomatic replacement of one mineral phase by another. During the recrystallization, the lattice of the dahllite-type hydroxyapatite gives way to the isomorphic series of francolite-type carbonate-fluorapatites. According to such interpretation, the intermediate values of lattice parameters, as well as carbonate-ion and fluorine contents, reflect a simultaneous presence of both phases. Therefore, the trends described above express an increase of the proportion of francolite-type apatite owing to the reduction of the dahllite-type variety.

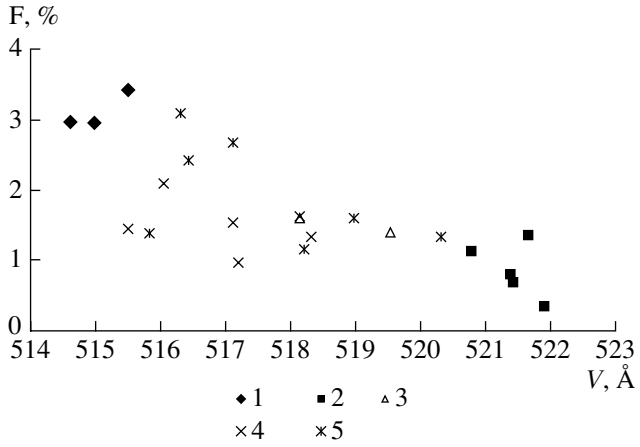

Fig. 7. Dependence of elementary cell volume (*V*) on the fluorine content in the studied samples. (1) Phosphorites; (2) fish teeth; (3) dreikanters; (4) fish bones; (5) whale bones.

The skeletal apatite recrystallization during fossilization (diagenesis) promotes the precipitation of an apatite variety with a lower OH-ion content (consequently, higher F content, as it follows from the stoichiometry) in the pore space of bone remains. Keeping in mind that primary skeletal apatites are represented by extremely fine-grained elementary crystallites, which are isolated from each other with organic matter films, at least, during the lifetime of organisms, we believe that the recrystallization takes place by small blocks. Therefore, if we measure by means of powder diffractometry the average content of strains in the specimen with a great number of diffracting crystallites, we obtain a dispersed pattern (Table 4). Measurements of lattice parameters also yield the same results (Fig. 2).

We suggest that rapid *post mortem* alterations in the skeletal mineral composition (e.g., in relationships between P, OH, CO_3, and Ca/P) lead to changes in the space group. Therefore, the formulas describing the hexagonal system are inapplicable here. Hence, we have to carefully treat some values given in Table 4. For example, crystallinity of a mineral with nanometer-sized crystallites theoretically must not differ from that of quartz.

The phosphate component in recent skeletons is always built up of prismatic crystals, whereas the habit of elementary crystallites in the altered bioapatites is random. We can also distinguish the enamel of modern ("fresh") teeth from their dentine by the size and habit of elementary crystallites.

CONCLUSIONS

The geochemical and mineralogical studies carried out on diverse bone remains of fishes and marine mammals from different regions of the World Ocean ranging from the Recent (including living shark teeth) to the Miocene make it possible to draw some conclusions concerning the specifics of bioapatite alteration during fossilization and diagenesis.

The mineral component appearing in the process of biomineralization of bone tissues and phosphatic lingulate shell is represented by the F–OH–CO_3-apatite (hydroxyfluorapatite-carbonate). The apatite is in the dynamic equilibrium with thermodynamic conditions existing within the parental organism during the origination in a living organism. The newly formed mineral phase consists of taxon-specific (in habit, size, and strain) crystallites. The formation of the mineral phase is controlled by nonlinear laws of biochemical reactions, which differ from the linear laws of equilibrium thermodynamics that govern the precipitation and diagenetic alteration of the carbonate-fluorapatite of oceanic phosphorites. The latter are evidently in equilibrium with thermodynamic conditions of the surrounding bottom or interstitial waters.

The data presented in this work show that the mineral phases appearing as a result of *post mortem* recrystallization of the skeletal apatite are not built up of primary bioapatite crystallites. Hence, changes in the primary composition and lattice parameters of the syngenetic skeletal apatite are also accompanied by the transformation of its crystal habit and lattice strains. The deviation from hexagonality reflected in the large scatter of lattice parameters and strains indicate a metastable state of the bioapatite. Consequently, skeletal apatites having such defects correspond to an immature recrystallization stage under thermodynamically nonequilibrium conditions (in the water–solid phase system).

Thermodynamic conditions, which existed in living tissues and maintained the metastable state of the dahllite-type apatite due to the living matter energy, disappear after the death of an organism. Adaptation to the new environment leads to changes in the bioapatite characteristics (chemical composition, crystallographic parameters, crystallite size, and lattice strains). The equilibration rate of depends on the medium of diagenesis and tissue type that undergoes fossilization or, more precisely, on the relationship between mineral (apatite) and organic matter components in the tissue. In bone tissues with the lowest organic matter content (e.g., fish teeth), the francolitization of bioapatite proceeds more slowly, and even the Miocene teeth preserve characteristics of the primary dahllite-type bioapatites. Deceleration of the process is also possibly related to a higher density of teeth as compared to porous bones. This hinders the penetration of reactive solution (bottom or interstitial water) to the apatite alteration microzone.

The chemical composition of bioapatite changes as a result of *in situ* recrystallization. The newly formed apatite does not contain hydroxyl-ion. Depending on the rate and scale of the process, the (sub)fossil bone material preserves for a while the mosaic mineral composition with the simultaneous presence of two apatite phases. The absence of continuous dahllite-to-francolite transition may mean that the fossilization represents a jump-type (stepwise) nonlinear process related to the removal of the bioenergy effect, i.e., transfer of the apatite from living matter to the bioinert state (according to V.I. Vernadsky). Fluorapatite with high carbonate-ion content is the final product of this process. The further development of the skeletal apatite is identical to the alteration of apatite in phosphorites during late phases of diagenesis.

ACKNOWLEDGMENTS

This work was supported by the ESF (grant no. 5275).

REFERENCES

Baturin, G.N., *Fosfority na dne okeanov* (Phosphorites on the Ocean Floor), Moscow: Nauka, 1978.

Bremner, J.M., Concretionary Phosphorite from SW Africa, *J. Geol. Soc.* (London), 1980, vol. 137, pp. 773–786.

Bremner, J.M. and Rogers, J., Phosphorite Deposits on the Namibian Continental Shelf, *Phosphate Deposits of the World. III Neogene to Modern Phosphorites*, Burnett, W.C. and Riggs, S.R., Eds., Port Chester: Cambridge Univ. Press, 1990, pp. 143–152.

Dahm, S. and Risnes, S., A Comparative Study of Hydroxide and Carbonate Adsorption Bands in Spectra of Shark Enameloid, Shark Dentin, and a Geological Apatite, *Calcif. Tissue Int.*, 1999, vol. 65, pp. 459–465.

Elliott, J.C., *Structure and Chemistry of the Apatites and Other Calcium Orthophosphates. Studies in Inorganic Chemistry 18*, Amsterdam: Elsevier, 1994.

Gulbrandsen, R.A., Relation of Carbon Dioxide Content of Apatite of the Phosphoric Formation to Regional Facies, *U.S. Geol. Surv. Prof. Pap.*, 1970, no. 700, pp. 9–13.

Gulbrandsen, R.A., Robertson, C.E., and Neil, S.T., Time and Crystallization of Apatite in Seawater, *Geochim. Cosmochim. Acta*, 1984, vol. 48, pp. 213–218.

Iveronova, V.I. and Revkevich, G.P., *Teoriya rasseyaniya rentgenovskikh luchei* (Theory of X-Ray Dispersion), Moscow: Mosk. Gos. Univ., 1978.

Kochenov, A.V. and Stolyarov, A.S., Problems of the Genesis of Manganese and Uranium–Rare Metal Ores in the Maikop Group, *Litol. Polezn. Iskop.*, 1996, vol. 31, no. 2, pp. 182–195 [*Lithol. Miner. Resour.*, 1996, vol. 31, no. 2, pp. 162–173].

Lucas, J. and Prévôt, L., Phosphates and Fossil Preservation, *Tophonomy: Releasing the Data Locked in the Fossil Record* Allison, P.A. and Briggs, D.E.G., Eds., New York: Plenum Press, 1991, pp. 389–409.

McClellan, G.H. and Lehr, J.R., Crystal Chemical Investigation of Natural Apatites, *Am. Mineral.*, 1969, vol. 54, pp. 1374–1391.

McConnell, D., *Apatite–Its Crystal Chemistry, Mineralogy, Utilization, and Geologic and Biologic Occurrences*, Vienna: Springer, 1973.

Murdmaa, I., Nemliher, J., Bogdanova, O., *et al.*, Ferromanganese and Phosphatic Hardgrounds on the Western Pacific Guyots Drilled during Legs 143 and 144, *Proc. ODP. Sci. Res*, 1995, vol. 144, pp. 413–428.

Nathan, Y., The Mineralogy and Geochemistry of Phosphorites, *Phosphate Minerals*, Nriagu, J.O. and Moore, P.B., Eds., Berlin: Springer, 1984, pp. 275–290.

Nemliher, J. and Kallaste, T., Secondary Alteration of the Shell Apatite of *Discinisca tenuis* from Luderlitz, Namibia, *Litol. Polezn. Iskop.*, 2002, vol. 37, no. 1, pp. 21–27 [*Lithol. Miner. Resour.* 2002, vol. 37, no. 1, pp. 18–24].

Nemliher, J. and Puura, I., Shell Mineralogy of Lingulate Brachiopods from the East Baltic Cambrian-Ordovician "Obolus Phosphate," *Proc. WOGOGOB Symp. Geol. Surv. of Demmark and Greenland*, 1996, no. 98, pp. 79–89.

Nemliher, J., Kallaste, T., and Puura, I., Hydroxyapatite Varieties in Recent Fish Scales, *Proc. Eston. Acad. Sci., Ser. Geol.*, 1997, vol. 4, pp. 187–196.

Nemliher, J., Laas, T., Kallaste, T., and Puura, I., Mineral Composition of the Dermal Skeleton of Devonian Fishes from Estonia, in *Proc. Eston. Acad. Sci., Ser. Geol.*, 1996, vol. 45, pp. 203–215.

Nriagu, J.O., Phosphate Minerals: Their Properties and General Modes of Occurence, *Phosphate Minerals*, Nriagu, J.O. and Moore, P.B., Eds., Berlin: Springer, 1984, pp. 8–107.

Schuffert, J.D., Kastner, M., Emanuele, D., and Jahnke, R.A., Carbonate-Ion Substitution in Francolite: A New Equation, *Geochim. Cosmochim. Acta*, 1990, vol. 54, pp. 2323–2328.

Sharkov, A.A., Specific Features of the Structure and Evolution of U-and REE-Bearing Organic Phosphate Deposits in the Southern Mangyshlak Region, *Litol. Polezn. Iskop.*, 2000, vol. 35, no. 3, pp. 290–307 [*Lithol. Miner. Resour.*, 2000, vol. 35, no. 3, pp. 252–266].